ELSEVIER

In Collaboration with
the Netherlands Institute for Sea Research

JOURNAL OF SEA RESEARCH

Journal of Sea Research 41 (1999) 35–53

Single particle analysis of suspended matter in the Makasar Strait and Flores Sea with particular reference to tin-bearing particles

V.M. Dekov [a,1], A. Van Put [a], D. Eisma [b], R. Van Grieken [a,*]

[a] *Department of Chemistry, University of Antwerp (UIA), Universiteitsplein 1, B-2610 Antwerp, Belgium*
[b] *Netherlands Institute for Sea Research, P.O. Box 59, NL-1790 AB Den Burg, Texel, Netherlands*

Received 15 December 1997; accepted 12 October 1998

Abstract

Suspended matter samples filtered from surface waters and two depth profiles from the Flores Sea and Makasar Strait were investigated by electron probe X-ray microanalysis (EPXMA) and laser microprobe mass analysis (LAMMA). EPXMA yielded discrete morphological and chemical analysis of the major particle types of suspended matter. Cluster analysis revealed that thirteen main particle types described the composition of suspended matter of the Flores Sea and Makasar Strait. Silicates, aluminosilicates and Fe-oxyhydroxides were the predominant particle types. Suspended matter of the basins studied contained high levels of tin-bearing particles. On the basis of their composition, tin particles can be divided into three groups: (1) tin oxide/hydroxides (cassiterite, romarchite, hydroromarchite); (2) iron-oxyhydroxides with adsorbed tin; and (3) mixed oxidation state tin hydroxysulphates. Only ultra-fine cassiterite particles enter the seawater in suspended state. Dissolved tin species entering the sea have three alternatives: (1) to be scavenged by Fe-oxyhydroxides; (2) to precipitate as tin oxide/hydroxides (romarchite, hydroromarchite); (3) to precipitate as tin hydroxysulphates. The conclusion is that dissolved and suspended tin originate from local sources in the land frame of the basins as well as from remote sources in the Indonesian Archipelago. Four different sectors of the waters studied have suspended matter with different composition: (1) the Mahakam River–Delta zone; (2) the open Flores Sea; (3) the landlocked Saleh Bay; (4) the Makasar Strait proper. The depth distribution of suspended particle types is mainly influenced by: (1) the bottom nepheloid layer and calcite lysocline in the Flores Sea; (2) the high bioproduction in the surface water layer and the vertical distribution of organic matter in the Makasar Strait.

Keywords: Makasar Strait; Flores Sea; suspended matter; tin

1. Introduction

In 1929–1930, the Snellius-I Expedition aboard HMS *Willebrord Snellius* for the first time investigated the hydrology, geology and biology of the Indonesian seas. Some 50 years later (1984–1985) its counterpart, the Snellius-II Expedition aboard RV *Tyro* continued to extend our knowledge on these seas and put new questions to the scientists. The Indonesian seas, which combine complex tectonic, active recent volcanism, tropical climate with a high rate of weathering, rich biota, and complicated hydrodynamics have no rivals elsewhere in the World Ocean. The discussions on some facets of these fea-

[1] Present address: Department of Geology and Paleontology, University of Sofia, 15 Tzar Osvoboditel Blvd., 1000 Sofia, Bulgaria.
* Corresponding author. Tel.: +32-3-820-2345; Fax: +32-3- 820-2376; E-mail: vgrieken@uia.ua.ac.be

1385-1101/99/$ – see front matter
PII: S1385-1101(98)00035-5

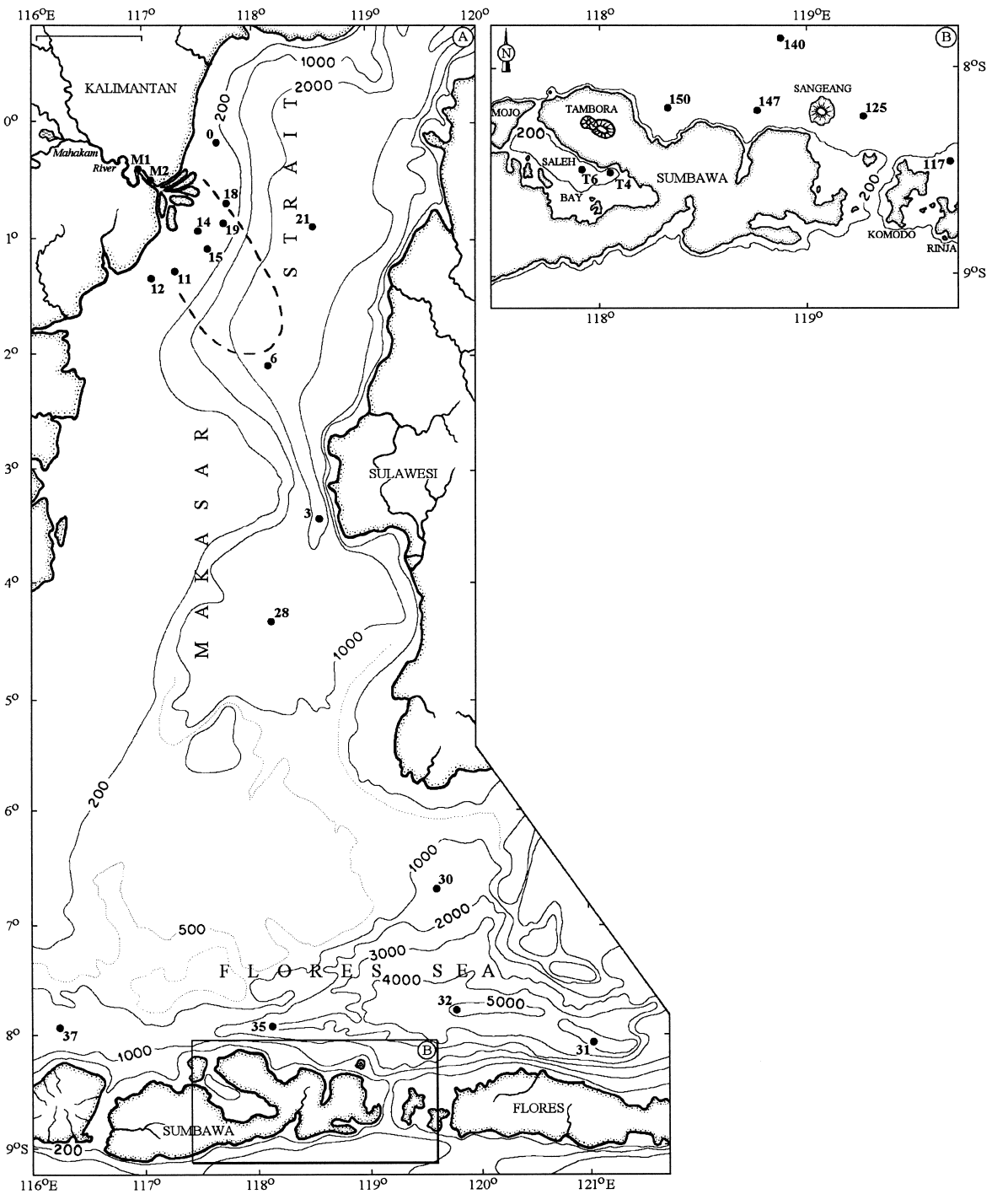

Fig. 1. (A) Map of study area, the Makasar Strait and Flores Sea. (B) Enlargement of part of the Island of Sumbawa and Saleh Bay. Dots = sampling stations; dashed line = Mahakam River plume of low salinity (S = 33.5‰, Eisma et al., 1989). Isobaths in metres. The bar in the upper left of (A) is 100 km long.

tures in the Proceedings of Snellius-II Symposium (Postma, 1988; Van der Land, 1989; Duinker and Everaarts, 1989; Van Hinte et al., 1989a,b; Zijlstra et al., 1990) give us a better knowledge of how this dynamic link between the Pacific and Indian Ocean works.

The Flores Sea is a typical back-arc basin surrounded by the inner-arc islands of Sumbawa and Flores (Sunda–Banda Tertiary volcano/plutonic arc) to the south and by the Island of Sulawesi to the north (Fig. 1). The Makasar Strait links this basin and the adjacent Bali and Java Seas with the Pacific Ocean waters through the Sulawesi Sea. The surface water flow patterns in this region vary from season to season (Fig. 2). The geology of the eastern Indonesian seas, which occupy a critical place in the complex zone between the Indian–Australian, Eurasian and the Philippine plates, has been discussed elsewhere (Curray, 1989; Katili, 1989). The evolution and resources of this Asia–Australian tungsten–tin metallogenic belt have been objects of many works (Kuo-Chin, 1995; Pei and Qiu, 1995; Supriyadi, 1996). In the Indonesian Archipelago, as a result of high tectono-magmatic activity, steep mountains and stormy rains, the major rivers have among the highest yields of suspended matter in the world. These islands deliver about 3×10^9 t yr^{-1} of suspended matter to the surrounding seas, much more than the well-known giant African and South American rivers, and have a sediment flux of >1000 t km^{-2} yr^{-1} (Milliman and Meade, 1983). The Mahakam River, one of the largest rivers on the Island of Kalimantan, discharges into the Makasar Strait where it has built up a large fan-shaped delta (Eisma, 1990).

Studying the dispersal of suspended matter and composition of sediments of the Makasar Strait and Flores Sea (Eisma et al., 1989, 1992), we came across intriguing features. The suspended matter contained varying amounts (in some cases considerable) of Sn-bearing particles. Tin, with its difficult analytical chemistry, seems to be a less attractive element for the geochemists dealing with marine chemistry and little has been published on it (Shimizu and Ogata, 1963; Hamaguchi et al., 1964; Smith and Burton, 1972; Brewer, 1975; Hamaguchi and Kuroda, 1978; Li, 1981; Galvin, 1996). Its behaviour in suspended form in the oceanic environment remains unclear to date.

The present paper is an addition to and an extension of a previous work (Eisma et al., 1989). It is an attempt to give some new details on the single particle groups of suspended matter from the

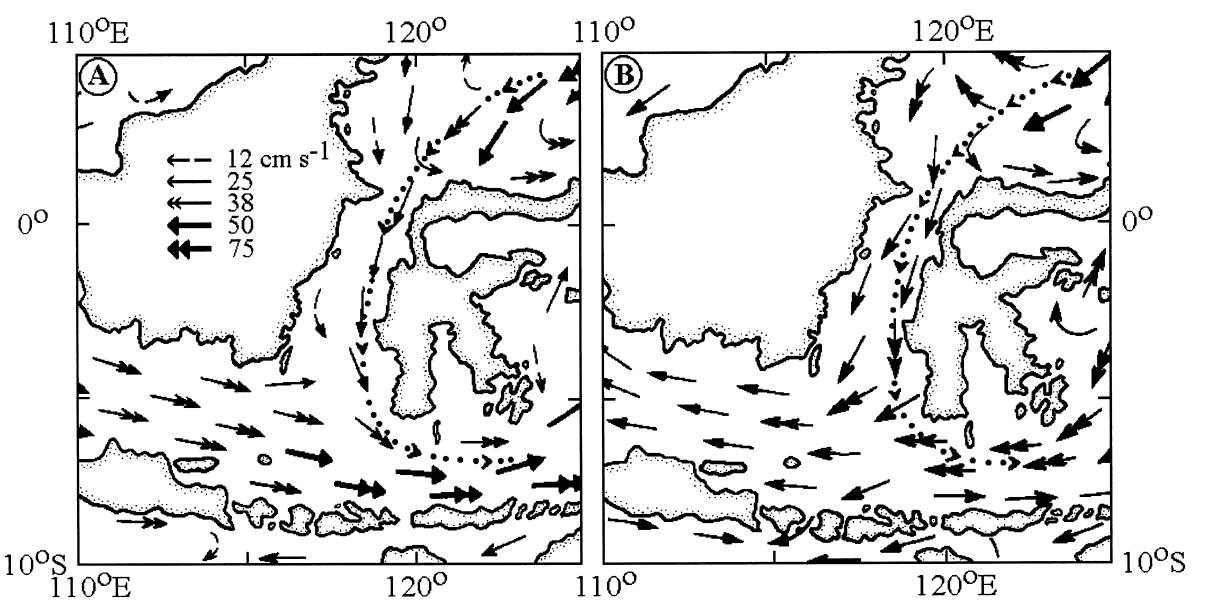

Fig. 2. Surface waters currents in the studied area during (A) February (wet season) and (B) June (dry season) (after Wyrtki, 1961). Dotted line = flow pattern of waters at 500–1000 m depth through the Makasar Strait and northern Flores Sea (after Van Bennekom, 1988).

Makasar Strait and Flores Sea, with an emphasis on the tin-bearing particles.

2. Material and methods of investigation

This work is based on suspended matter samples (total of 42) collected in the Makasar Strait and Flores Sea with the Dutch RV *Tyro* in November 1984 (wet season) and with the German RV *Sonne* in September–October 1986 (dry season). The sample set collected by RV *Sonne* covers the waters off the Island of Sumbawa (Fig. 1B), which shows recent volcanic activity (last eruptions of Tambora volcano: 1815; and of Sangeang: 1964, 1986). To identify the chemical characteristics of river-borne suspended matter, two samples (M1 and M2) were collected upstream in the Mahakam River, well out of the range of marine influence. Samples T4 and T6 were taken in the Saleh Bay, a semi-enclosed basin on the Island of Sumbawa near to the Tambora volcano.

Two depth profiles were sampled: one in the Makasar Strait off Sulawesi (site #6, 2600 m depth), and another in the deepest part of the Flores Sea (site #32, 5037 m depth). All the other samples were taken from the surface waters (Fig. 1).

Water samples were collected with 30 dm^3 Niskin bottles mounted on a Rosette sampler. Subsamples (up to 100 cm^3) were filtered over 0.4 μm pore-size Nuclepore filters. Prior to storage the samples were washed successively with 40%, 70% and 90% of ethanol to dehydrate the organic material and to remove the seasalts. After drying, the filters were mounted on plastic rings and coated with carbon. Scanning electron microscopy (SEM), automated electron probe X-ray microanalysis and laser microprobe mass analysis were applied to suspended matter specimens using the methods already described (Bernard et al., 1986; Wouters et al., 1988a).

The relative intensities of the K_α lines of Na, Mg, Al, Si, S, K, Ca, Ti, Mn and Fe were used to classify the particles into specific groups (Bernard et al., 1986). First a hierarchical cluster analysis (Massart and Kaufman, 1983), using Ward's method to calculate object distances, was performed for each sample to obtain specific particle groups and the mean X-ray intensities in each group in a sample. Then, hierarchical cluster analysis was done again, but this time all groups obtained previously were clustered to get a set of centroids (training vectors) for non-hierarchical cluster analysis over all particles of all samples (Forgy, 1965). After non-hierarchical clustering, the average relative X-ray intensities of the detected particle types were converted into abundances of appropriate elements by applying a ZAF correction procedure (Van Borm and Adams, 1988). Finally the abundances of some elements, when relevant, were recalculated to their oxide forms. For each particle type, the general mean abundance, average diameter, and shape factor were calculated for all samples. Also the abundances of the groups in the individual samples were measured.

Prior to analysis, measurements on a tin standard were made to determine the Sn L_α/L_β intensity ratio, so that a correction could be made for possible overlapping of the L_β peak for Sn and the K_α peak for Ca.

3. Results and discussion

3.1. Suspended particle types

Thirteen representative particle types were selected to evaluate the dispersal of suspended matter in the region studied, on the basis of the abundance distribution of these groups (Table 1).

The first three groups (Table 1) contributed almost 50% of all the particles. XRD analyses of bottom sediments and sediment trap samples (Eisma et al., 1989) indicated that quartz, micas, chlorite, smectites, feldspar and amphibole were commonly present. Apparently, group #1 (Table 1) include Si-rich particles: quartz, opal. Opaline particles could have a volcanogenic and/or biogenic nature. Recent volcanic activity and high bioproduction in this region (Van der Land, 1989; Van Hinte et al., 1989a,b) are able to supply a considerable flux of opaline silica. Moreover, SEM observations often indicated clusters of diatoms. Hence, the genesis of the most abundant particle type, quartz–opaline, is rather complex: terrigenous–volcanogenic–biogenic.

The two aluminosilicate groups (#2 and #3) differ in their composition. While group #2 probably represents micas and feldspars (Si–Al composition with

Table 1
Average composition and relative abundance (in wt.%) of the particle types identified for the suspended matter surface samples from the Mahakam River, Makasar Strait and Flores Sea

Group	Particle type	Abundance (%)	Na_2O	MgO	Al_2O_3	SiO_2	P	S	K_2O	CaO	TiO_2	MnO_2	Fe_2O_3	SnO_2	EQDIA [a] (μm)	SF [b]
1	Si	18	0.3 (1.2) [c]	0.1 (1.4)	0.7 (2.7)	97 (6)	0 (0)	0.1 (1.6)	0.2 (1.4)	0.4 (2.4)	0.3 (1.5)	0 (0.1)	0.8 (2.5)	0.1 (1.3)	2.2 (2.2)	2.0 (2.1)
2	Si–Al (Fe)	17	1 (3)	0.2 (1.6)	30 (9)	59 (8)	0 (1.9)	0.2 (3.4)	2 (6)	0.6 (3.0)	0.4 (3.0)	0 (0)	6 (5)	0.4 (2.9)	2.3 (2.2)	1.9 (1.1)
3	Si–Fe–Al	7	1 (4)	1 (4)	17 (10)	43 (10)	0.1 (2.4)	2 (9)	0.5 (2.9)	3 (9)	3 (8)	0 (0.3)	28 (12)	2 (6)	2.4 (2.0)	2.2 (1.6)
4	Ca (Mg)	2	2 (5)	7 (9)	0.6 (2.2)	3 (6)	0.5 (5.8)	1 (5)	0.2 (2.4)	85 (14)	0 (0)	0 (0)	2 (4)	0 (0)	2.2 (2.5)	2.4 (2.0)
5	Ca–S	14	3 (3)	0.4 (1.2)	0.2 (1.0)	1 (4)	0 (0)	38 (7)	0.8 (1.4)	54 (7)	0.2 (1.8)	0 (0.2)	1 (4)	1 (3)	2.8 (6.4)	3.5 (7.2)
6	Fe	13	0.3 (1.6)	0.1 (0.7)	0.1 (1.5)	2 (4)	0 (0.9)	1 (4)	0 (0.2)	0.2 (2.3)	0.1 (1.0)	0.1 (0.7)	96 (7)	0.8 (3.0)	1.7 (2.1)	1.6 (0.6)
7	Fe–Sn (Si)	6	3 (6)	0.3 (1.9)	3 (7)	11 (13)	0.3 (3.6)	2 (9)	0 (0.5)	3 (7)	0.7 (4.3)	0.1 (0.9)	66 (10)	12 (15)	1.6 (1.7)	1.9 (2.3)
8	Sn–Fe	8	0 (0.4)	0 (0.4)	0.3 (2.5)	1 (7)	0.3 (3.9)	1 (9)	0 (0)	4 (8)	0 (0)	0 (0)	16 (14)	78 (16)	1.3 (1.6)	2.0 (1.2)
9	S–Sn (Na)	3	12 (8)	0.2 (0.8)	0.3 (1.5)	4 (8)	0.1 (3.2)	40 (18)	0 (0)	4 (7)	0.1 (1.2)	0 (0)	8 (12)	31 (18)	1.8 (2.1)	2.4 (2.4)
10	Ti (Fe)	3	0 (0)	0 (0)	2 (5)	8 (11)	0 (0)	4 (16)	0 (0)	0.2 (1.6)	80 (19)	0 (0.2)	5 (8)	0.5 (3.5)	1.0 (1.2)	1.5 (0.7)
11	Al	0.5	1 (2)	0 (0)	83 (20)	4 (10)	3 (14)	4 (11)	0.2 (2.2)	1 (4)	3 (9)	0 (0)	0.4 (1.2)	0 (0)	3.8 (5.2)	2.2 (1.9)
12	Na	6	99 (9)	0 (0)	0 (0)	0.6 (5.8)	0 (0)	0.1 (1.8)	0 (0)	0.2 (4.4)	0 (0)	0 (0)	0.4 (4.0)	0.1 (2.6)	1.3 (0.9)	1.4 (0.4)
13	Na–S	3	67 (12)	1 (5)	0 (0)	2 (8)	0 (0)	18 (17)	1 (5)	4 (11)	0.1 (1.5)	0 (0)	7 (12)	1 (5)	2.1 (3.0)	2.0 (1.4)

[a] Equivalent spherical diameter. [b] Shape factor. [c] Standard deviation.

some Fe and K), group #3 includes clearly Fe-rich clay minerals: montmorillonite and nontronite.

Aggregates of aluminosilicate and biogenic fragments were commonly observed during our SEM studies. These flocs amalgamated different types of particles (quartz, aluminosilicate and iron-rich particles, etc.), range between 10 and 50 μm and generally have a densely packed structure. Analysis of the organic matter which holds together the flocs showed that it was of marine origin, even for flocs in the Mahakam River plume (sites #14, #15) (Eisma et al., 1989). Hence, the flocs are formed in situ and have not been supplied from land.

The abundant group #6 (13%) most likely contains amorphous and poorly crystallised Fe-oxyhydroxides, mainly goethite (Lisitzin, 1972). The particle groups #10, #4 and #11 display low overall abundance. Therefore, we can restrict ourselves almost solely to assigning them to a rutile group (rutile, brookite, anatase), a calcite/dolomite and a gibbsite group, respectively. The occurrence of titanium oxide minerals and aluminium hydrates (gibbsite) is not surprising in such geologic and climatic settings. Foraminiferal tests and coccoliths (both with $CaCO_3$ skeletal elements) are common constituents of the suspended matter in the region (SEM observations).

The Na–S particles (group #13) and the Na-rich group (#12) (actually NaCl, because Cl was not a selected element) were most likely results of incomplete removal of seawater.

An interesting feature of the samples studied is the presence of Sn-rich particles, making up as much as 17% of a compilation of three different Sn associations. However, in some cases (site #21), the Sn-bearing particles can make up as much as 81% of the particles analysed.

The most abundant tin particle type (group #8) is the tin oxide/iron-oxyhydroxide mineral group. Tin oxide minerals are comparatively few. Cassiterite (SnO_2) could explain the chemical composition of this group. It is a typical resistate, representing the chemically unchanged residue from weathering. In its crystal lattice, iron (Fe^{3+}, Fe^{2+}) is usually present either as isomorphous admixtures substituting for tin (up to about Fe:Sn = 1:6) or as products of disintegration of solid solutions. The presence of cassiterite in the marine suspended matter of this area is not fully unexpected. This region is one of the world's

main producers of tin (Kuo-Chin, 1995; Supriyadi, 1996) and the extensive mining of alluvial placers and coastal waters in Thailand, Malaya and at the Tin Islands (Singkep, Bankga and Belitung) could provide cassiterite-containing suspension in the mine tailings dispersing far away from the coast. Although cassiterite is a heavy mineral, the favourable direction and velocity of the surface currents during the sampling campaign (Fig. 2A) would make possible the transport of micrometre-sized particles (in general $\sim$1 μm) in suspended state as far as the basins studied (>1500 km eastward). Moreover, the tin content in the suspended matter increases eastward, throughout the Java Sea towards the Flores Sea: 0.45% in the western Java Sea, south of Belitung Island; 0.89% in the central Java Sea, south of Kalimantan Island; 1.76% in the Bali Sea, near the Flores Basin (Van der Sloot et al., 1987). These observations have two possible explanations. (1) The cassiterite particles have a far-away source, probably the Tin Islands. Coastal mining there produces cassiterite-containing suspension relatively rich in organic matter. Much of the sedimentary organic matter is intimately associated with the surfaces of detrital minerals (Ransom et al., 1998). During its transportation eastward, the suspended organic matter decays releasing more resistant phases unaffected. This leads to a relative enrichment of suspended matter in the remaining particles eastward. (2) The suspended cassiterite has local sources in the frame of the basins studied. There are, indeed, a few indications for Sn-containing placers in southeast Kalimantan (Stumpfl and Clark, 1965).

Cassiterite, the most important tin mineral, is chemically resistant to weathering. However, some tin is mobilised during the weathering cycle and dissolved in natural waters. Once weathered, tin goes into solution and its further fate is mainly governed by oxidation-reduction conditions. In natural waters tin behaves in different ways according to its oxidation state (Hamaguchi and Kuroda, 1978). Quadrivalent tin has a high ionic potential and is thought to precipitate promptly into hydrolysates along with aluminium. Divalent tin has a low ionic potential and during rock weathering goes into solution as cations. However, in order to survive in the form of stable ions, an acidic environment must prevail for the Sn^{2+}. Therefore, complex tin ions may be expected to be stable ionic species in the river waters flowing to the ocean. In the oxygenated seawater, tin behaves non-conservatively and its probable main species is $SnO(OH_3)^-$ (Kennish, 1994). Going from a coastal to an open oceanic environment the dissolved tin sharply decreases (Smith and Burton, 1972). This suggests that in coastal regions a rapid removal of tin from the seawater occurs, a notion consistent with the moderate residence time of tin in the ocean (5×10^5 yr; Kennish, 1994, p. 117).

The investigations on the stability of secondary tin minerals (Edwards et al., 1992, 1996) suggest that in seawater romarchite (SnO) and its hydrated form hydroromarchite ($3SnO{\cdot}H_2O$) are the minerals which should precipitate from tin chloride, sulphate and hydrous ions. Hence, group #8 obviously encompasses cassiterite, romarchite and hydroromarchite.

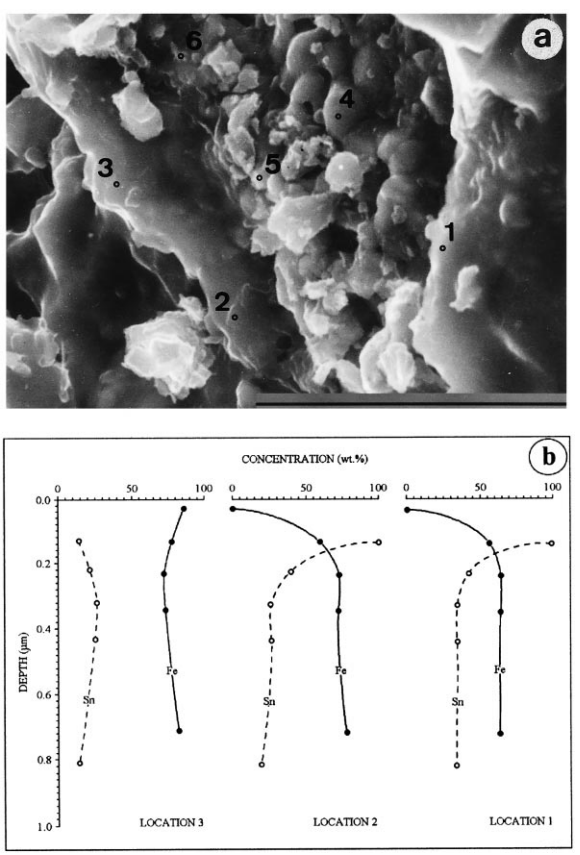

Fig. 3. (a) Secondary electron image of a Fe–Sn particle (group #7); open dots = locations of the point analyses; scale bar equal to 10 μm. (b) Depth profiles of iron and tin at three locations of the particle shown in (a).

Tin occurs in many sulphide ores in the form of relatively pure tin sulphides (SnS, SnS_2, Sn_2S_3). However, tin sulphide particles could not be stable phases in the marine environment and it is not likely that tin sulphides are present in group #9 (Table 1). In view of the solution chemistry of tin and the conditions in a natural saline environment (e.g. seawater) the mixed oxidation state tin hydroxysulphate ($Sn_7(OH)_{12}(SO_4)_2$) would be a thermodynamically stable phase (Edwards et al., 1996).

Another pathway of dissolved tin species in seawater is their removal from the solution by adsorption onto, or co-precipitation along with, abundant and efficient scavengers such as iron-oxyhydroxides. Isomorphous replacement of iron by tin (IV) in goethite (α-FeOOH) or in other FeOOH might occur. The ionic radii of tin (IV) (0.71–0.74 Å) and iron (III) (0.67 Å) (Heydemann, 1969) are sufficiently similar to permit ready substitution. That is why we consider the Fe–Sn (Si) particle type (group #7, Table 1) to consist of iron-oxyhydroxides with scavenged tin. The Fe–Sn-rich particles display, in general, crusty forms (Fig. 3a). The large size of these particles allowed us to obtain some additional information on their in-depth and lateral homogeneity, which was impossible for the Sn–Fe particles (group #8). For this purpose, energy-dispersive X-ray spectra were collected at different locations of the particles (Fig. 3a). The depth profiles (Fig. 3b) were obtained by applying gradually increasing voltages for X-ray generation. Both in-depth and lateral spectrum data were converted by the ZAF-procedure, integrating the different accelerating voltages in the case of the depth profiling, to obtain normalised weight fractions of the different elements detected. The results (Table 2; Fig. 3b) give an integrated picture on the distribution of Sn and Fe in the particle. It becomes clear that tin is more enriched in the surface layer and near the edges of the particle.

Natural mobilisation of tin during weathering is accelerated, however, by human activities in the area studied. The exploitation of the tin ore deposits exposes large quantities of waste rock to weathering. Thus, the riverine and coastal waters near mine tailings could contain high levels of man-mediated tin (Yim, 1981; Chansang, 1988). Although mine tailing seems to support appreciable amounts of tin to the basins of the region, the possibility of anthropogenic tin contamination, by ship, during sampling was not excluded and had to be investigated.

Table 2
Depth and lateral homogeneity for the Fe–Sn particle (in wt.%) represented in Fig. 3a

Voltage (keV)	Location 1		2		3		4		5		6	
	Fe	Sn	Fe	Sn	Fe	Sn	Fe	Sn	Fe	Sn	Fe	Sn
20	65	35	79	21	84	16	78	22	62	38	77	23
14	65	35	73	27	74	26	–	–	–	–	–	–
12	65	35	73	27	73	27	–	–	–	–	–	–
10	57	43	60	40	78	22	–	–	–	–	–	–
8	–	100	0	100	85	15	–	–	–	–	–	–

Actually tin, more specifically tributyltin, is a major component of antifouling paints, which are commonly used to cover the hulls of vessels to avoid attachment of aqueous organisms and subsequent increased running costs (Blundel and Evans, 1990). LAMMA has been applied to address this problem. This technique not only offers better speciation capabilities than EPXMA, it also accommodates additional information on organic constituents. Therefore, LAMMA was chosen to provide unambiguous proof that the Sn-rich particles in our samples are actually not tributyltin antifouling contamination particles.

LAMMA of selected Sn-rich particles from the suspended matter specimens and Sn-paint revealed that there is a clear-cut difference (Fig. 4). The most obvious difference is the regular occurrence of iron in the marine tin particle spectra (Fig. 4A+). The iron isotope pattern cannot unambiguously be detected in the paint spectra (Fig. 4B+). Furthermore, as expected, paint spectra exhibit more organic fragmentation peaks. The clearly higher relative intensities of phosphate peaks in the negative-mode spectra for the marine particles (Fig. 4A−) are not conclusive: earlier LAMMA on aquatic suspension particles (Wouters et al., 1988a) showed that every particle type exhibits such peaks. Moreover, they always appear in the so-called desorption mode (i.e. recorded at low irradiances without visible damage of the particle), which is loosely indicative of the surface layer of the particle. Most likely phosphate-containing compounds are adsorbed from the water

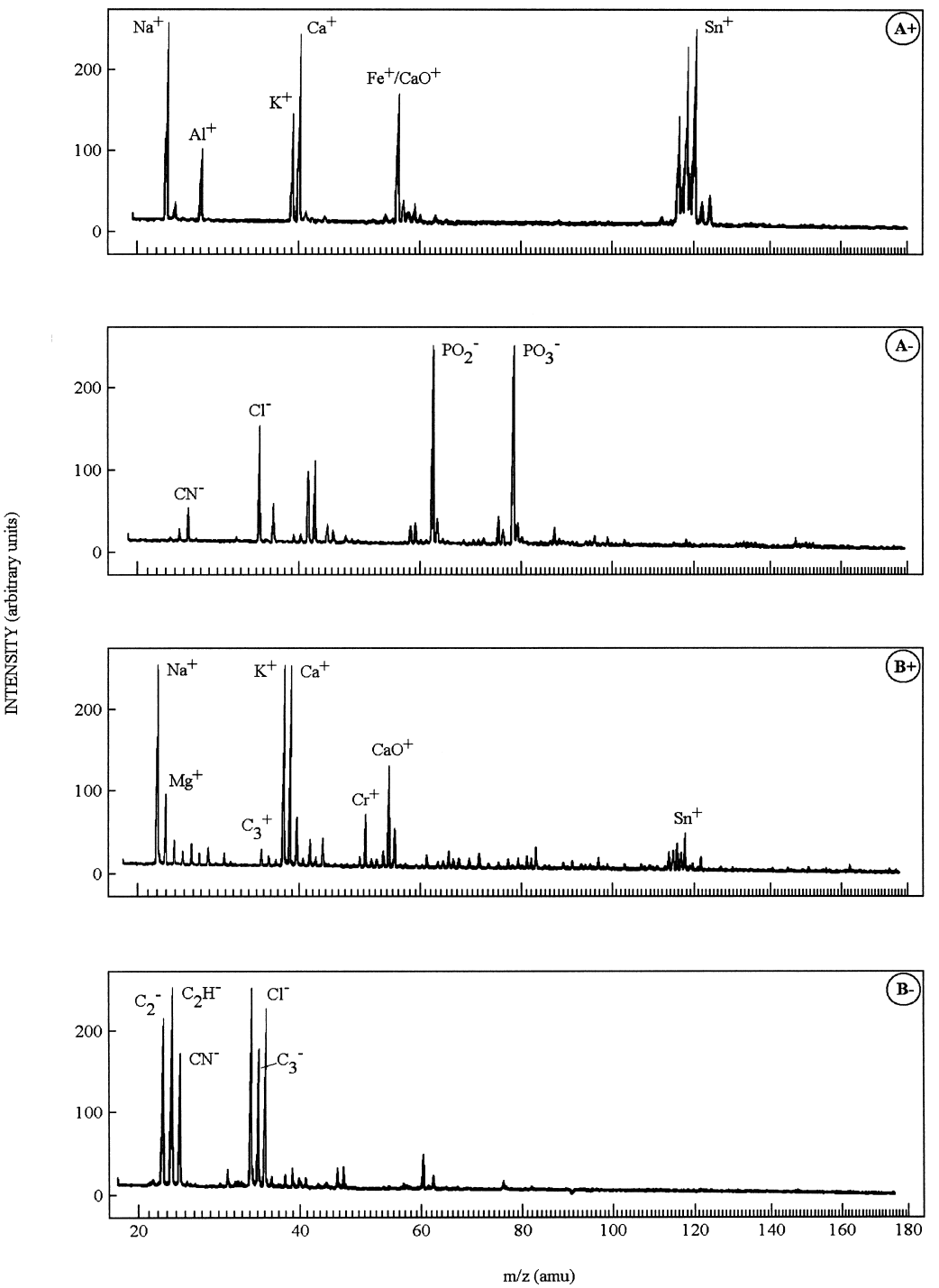

Fig. 4. Positive (+) and negative (−) mode LAMMA spectra of: (A) Sn–Fe particle representative for group #8; (B) paint chip containing tributyltin.

column. A comparison with LAMMA spectra obtained earlier for some tin compounds (Gucer et al., 1989) indicates that the isotope intensities found for the Sn particle (group #8) agree reasonably with the values for tin oxides. However, no diagnostic distinction can be made between SnO and SnO_2. Nevertheless, these results confirm that most of the tin present in this particle type can be classified as tin oxides.

Although applied successfully in the past (Wouters et al., 1988b) on similar and other types of samples (Otten et al., 1986), it was impossible to obtain indications about the surface coating of the Fe–Sn particles (group #7) from the LAMMA spectra recorded in the laser desorption mode. Consequently, the hypothesis postulated after the EPXMA depth profiling that Sn is present mostly at the surface of the Fe–Sn particles could unfortunately not be verified by the use of LAMMA.

The average contribution of the $CaSO_4$ particles (group #5) amounts to 14%. The gypsum particles (star-shaped or elongated in general) could result from an artefact during sample preparation by evaporation of seawater and by mixing seawater with ethanol (rinsing solvent). This could be derived from the results obtained from a filtration/rinsing experiment on filtered artificial seawater. The experiment was executed so that, in one case, complete filtration of an artificial seawater sample was allowed to take place before washing with twice-distilled water or ethanol. In the second case, the artificial seawater was allowed to mix with the rinsing solvent in the final stage of the filtration. The results showed that only when artificial seawater mixes with ethanol, are the typical star-shaped gypsum particles recovered.

The question remained whether the particles found in our samples were solely an effect of seasalt crystallisation. In the Atlantic deep waters (Lal, 1977) and Loire estuary (Ottmann and Shi, 1988), authigenic or syngenetic gypsum particles have been found. A second experiment was therefore conducted as an attempt to elucidate this question further. Principally, the experiment was based on the comparison of the maximum amount of gypsum that can possibly crystallise by evaporation of a residual water layer on the filter (after filtration), with the experimentally detected amount of gypsum for some samples. In the first stage of the experiment, the average volume of a residual water layer was determined by weighing several Nuclepore filters before and after filtration. From this volume, the maximum mass of gypsum/field that can crystallise, based on the composition of seawater (Riley and Chester, 1971), was calculated. This value was then compared with the experimental mass of gypsum recovered per field for some samples with a high abundance of gypsum particles. The results were not in good mutual agreement and indicated that the bulk of gypsum particles encountered were very likely formed by crystallisation of dissolved seasalts on the filters.

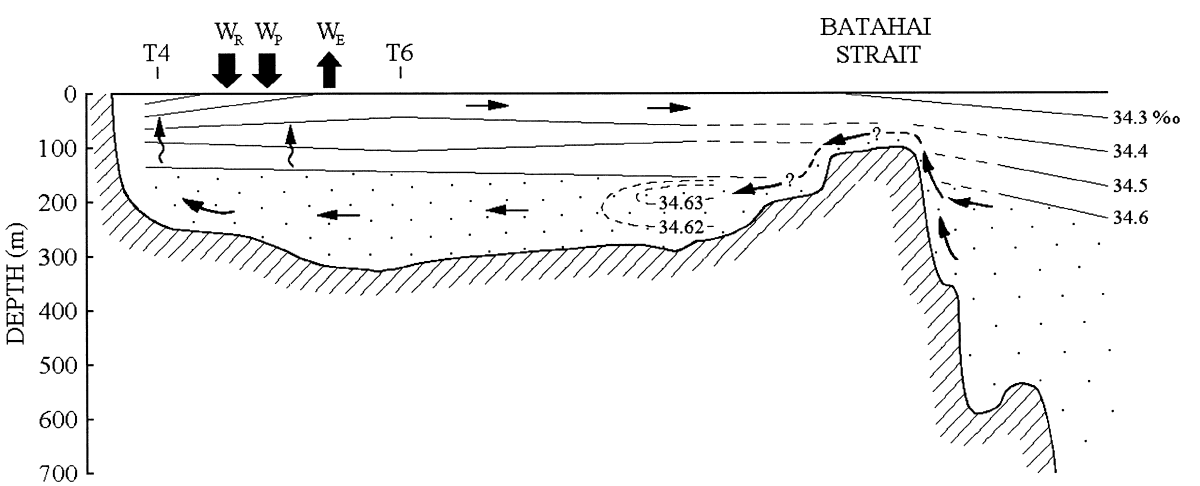

Fig. 5. Schematic section through the central part of the semi-enclosed Saleh Bay with distribution of the salinity (after Degens and Buch, 1989).

Table 3
Relative abundance distribution (in %) of the different particle types for the samples from the Mahakam River, Makasar Strait and Flores Sea

Group	Particle type	Mahakam River, Delta, and surface low-salinity plume									Makasar Strait				Flores Sea									Saleh Bay	
		M1	M2	14	15	0	18	19	11	12	6	3	21	28	30	31	117	125	140	147	150	35	37	T4	T6
1	Si	41	39	40	39	24	27	6	12	34	14	59	2.5	15	21	16	0.9	1.7	10	4	0	3	0.7	0.4	13
		(3)[a]	(3)	(5)	(3)	(3)	(3)	(2)	(2)	(3)	(2)	(3)	(0.9)	(2)	(3)	(3)	(0.9)	(0.8)	(2)	(2)	(0)	(1)	(0.5)	(0.4)	(3)
2	Si–Al (Fe)	36	35	39	20	49	46	7	18	19	26	27	3	13	25	10	0.9	3	7	10	2	3	1.1	0	16
		(3)	(3)	(5)	(3)	(3)	(3)	(2)	(2)	(2)	(3)	(3)	(1)	(2)	(3)	(2)	(0.9)	(1)	(2)	(3)	(1)	(1)	(0.6)	(0)	(3)
3	Si–Fe–Al	10	10	12	5	17	11	6	8	10	12	4	1.8	8	11	9	0.9	5	10	0	0	4	1.4	0.4	10
		(2)	(2)	(3)	(1)	(2)	(2)	(2)	(2)	(2)	(2)	(1)	(0.8)	(2)	(2)	(2)	(0.9)	(1)	(2)	(0)	(0)	(2)	(0.7)	(0.4)	(3)
4	Ca (Mg)	0	0	0	0.8	1	1.1	0.4	4	2.2	1	0	0.7	5	2	0	0	2.1	16	4	0	2	0.4	0	0
		(0)	(0)	(0)	(0.6)	(0.6)	(0.6)	(0.4)	(1)	(0.9)	(0.6)	(0)	(0.5)	(1)	(1)	(0)	(0)	(0.8)	(3)	(2)	(0)	(1)	(0.4)	(0)	(0)
5	Ca–S	0	0	3	4	0.3	3	2.3	2	3	10	0	0	0	0	39	4	24	4	24	56	2	58	77	11
		(0)	(0)	(2)	(1)	(0.3)	(1)	(0.9)	(1)	(1)	(2)	(0)	(0)	(0)	(0)	(4)	(2)	(3)	(1)	(5)	(5)	(1)	(3)	(3)	(3)
6	Fe	2	2.4	2	12	4	3	32	13	13	27	4	11	25	13	9	2	47	21	9	3	37	1.1	0.4	22
		(0.8)	(0.9)	(1)	(2)	(1)	(1)	(3)	(2)	(2)	(3)	(1)	(2)	(3)	(2)	(2)	(1)	(3)	(3)	(3)	(2)	(4)	(0.6)	(0.4)	(4)
7	Fe–Sn (Si)	7	7	1	5	2	4	20	6	5	7	2	11	10	8	10	0	8	8	6	0.9	8	1.1	0.4	9
		(1)	(2)	(1)	(1)	(0.8)	(1)	(3)	(1)	(1)	(2)	(0.8)	(2)	(2)	(2)	(2)	(0)	(2)	(2)	(3)	(0.9)	(2)	(0.6)	(0.4)	(3)
8	Sn–Fe	0.7	0	0	9	1	0.4	21	31	8	0	0.3	70	18	6	4	0	0.4	0	0	0	2	8	2	11
		(0.5)	(0)	(0)	(2)	(0.6)	(0.4)	(3)	(3)	(2)	(0)	(0.3)	(3)	(2)	(1)	(2)	(0)	(0.4)	(0)	(0)	(0)	(1)	(2)	(1)	(3)
9	S–Sn (Na)	0.3	0.3	0	1.2	0.7	1.1	0.8	3	1.1	0.4	0.7	0	0.8	4	1.1	0	3	0.9	1	0	2	27	19	0.8
		(0.3)	(0.3)	(0)	(0.7)	(0.5)	(0.6)	(0.5)	(1)	(0.6)	(0.4)	(0.5)	(0)	(0.5)	(1)	(0.8)	(0)	(1)	(0.7)	(1)	(0)	(1)	(3)	(3)	(0.8)
10	Ti (Fe)	4	5	2	3	1.3	2.5	1.9	3	4	2	3	1.1	3	8	1.1	0.9	1.7	6	1	0	2	0	0	6
		(1)	(1)	(1)	(1)	(0.7)	(0.9)	(0.9)	(1)	(1)	(0.8)	(1)	(0.6)	(1)	(2)	(0.8)	(0.9)	(0.8)	(2)	(1)	(0)	(1)	(0)	(0)	(2)
11	Al	0.3	0.7	0	0.8	0	0.7	0.4	0	1.1	0	0.3	0	1.9	0	1.1	0	0	3	0	0	0.6	0.4	0	0
		(0.3)	(0.5)	(0)	(0.6)	(0)	(0.5)	(0.9)	(0)	(0.6)	(0)	(0.3)	(0)	(0.9)	(0)	(0.8)	(0)	(0)	(1)	(0)	(0)	(0.6)	(0.4)	(0)	(0)
12	Na	0	0	0	0	0	0	1.1	0	0	0	0	0	0	0	0	78	2.4	10	29	23	0.6	0	0	0
		(0)	(0)	(0)	(0)	(0)	(0)	(0.7)	(0)	(0)	(0)	(0)	(0)	(0)	(0)	(0)	(4)	(0.9)	(2)	(5)	(4)	(0.6)	(0)	(0)	(0)
13	Na–S	0	0	0	0	0	0.4	0	0	0	0.4	0	0	0	0	0	11	3	3	11	11	34	0	0	0
		(0)	(0)	(0)	(0)	(0)	(0.4)	(0)	(0)	(0)	(0.4)	(0)	(0)	(0)	(0)	(0)	(3)	(1)	(1)	(4)	(3)	(4)	(0)	(0)	(0)

[a] Standard deviation.

However, the strikingly high amount of gypsum crystals in the Saleh Bay sample (T4, 2300 $pg/field_{exp}$. vs. 5 $pg/field_{theor}$.) raises the question whether the gypsum precipitation is geochemically possible in such an environment.

The Saleh Bay (Fig. 1B) is a small marine inlet with a two-layered stratified water column (Fig. 5). A distinct halocline has been established in mid-water and the vertical patterns of dissolved oxygen, water temperature and pH exhibit sharp gradients (Degens and Buch, 1989). The rise of Mojo Island (Fig. 1B), 25,000 yr ago (Degens and Buch, 1989) locked the basin and restricted the seawater inflow through two narrow and shallow channels. The Saleh Bay became a poorly ventilated basin with a stratified water body. During the sampling campaign, at the beginning of the wet season, the Saleh Bay should have a positive water balance: the combined rates of precipitation (W_P) and river input from the surrounding drainage area (W_R) exceed that of removal by evaporation (W_E). The surface layers of the basin have lower salinities and this produces an outflow of the low-salinity water into the adjacent ocean (Fig. 5). We suppose that under such circumstances, during intermittent upwellings from the lower, more saline water stage, the surface waters could locally turn out more saturated in $CaSO_4$. Consequently, the Saleh Bay samples give more gypsum artefacts than the other samples as a result of incomplete $CaSO_4$ removal through laboratory treatments.

3.2. Features of the lateral dispersal of suspended matter

We have examined the relative abundance distribution of the 13 representative groups for the surface-water suspended-matter samples for the Mahakam River, Makasar Strait, Flores Sea and Saleh Bay (Table 3; Fig. 6). Since the river input stretches far southeast (~400 km, Eisma et al., 1989) into the Makasar Strait, we discuss this zone of river water/seawater mixing: river, delta and surface low-salinity plume.

The spatial distribution of the *silica group* (#1, Fig. 6) exhibits some interesting features. The highest concentrations of this group are in the zone of mixing of the Mahakam River water with seawater. The silica content in the suspended matter drops away from the zone of the river influence towards to the open strait waters (site #6). The coastal waters of the Island of Sulawesi also have enhanced levels of silica (site #3). Flores Sea suspended matter has very low silica concentrations (Table 3; Fig. 6). SEM studies showed that the most frequent silica phase was detrital quartz; diatom skeletons were rare. Obviously, the main part of this particle type is supplied from the landmasses by rivers and streams, and is terrigenous (mostly quartz). We have no direct proofs about the role of volcanogenic silica. It is expected to contribute in the Flores Basin, off the Sunda–Banda inner volcanic arc. The biogenic factor (diatoms, etc.) is obviously not the main silica source. A remarkable feature is that the seafloor beneath the surface waters with a high silica content in the suspended matter is covered with terrigenous sediments (Fig. 7). Volcanogenic sediments underlie the sites with the lowest SiO_2 concentrations.

The *aluminosilicate group* (#2) is terrigenous with the highest levels in the zone of Mahakam River influence and with a minimum content in the southern Flores Sea (Fig. 6). Comparable results have been obtained for two other Indonesian rivers, the Solo and the Porong, discharging in the Strait of Madura, Java Sea (Hoekstra et al., 1989; Nolting et al., 1989).

The *iron-aluminosilicate particle type* (#3) exhibits an even distribution (Fig. 6) in the areas studied, implying that this type consists of Fe-clay minerals formed during alteration of the basic magmatic rocks which are widespread in the land frame of the waters studied.

Gypsum particles (#5) seem to be most abundant in the southern Flores Sea, close to the Island of Sumbawa.

The high correlation ($r = 91$) between the *iron-oxyhydroxide* (#6) and *Fe–Sn* (#7) particle types (Fig. 6) proves the hypothesis that the tin in group #7 is sorbed on the Fe-oxyhydroxide particles. On this basis (8% Fe–Sn particles vs. 13% Fe-rich particles) it can be concluded that some 20% of the particles formed a suitable substrate for considerable tin adsorption. The presence of tin in some of the other particle types (Table 1) and the excess of efficient scavengers (clays, oxyhydroxides: groups #2, #3, #6) demonstrate that obviously all the available tin dissolved in the waters studied has been scavenged.

The *tin oxide/hydroxide group* (Tables 1 and 3, #8; Fig. 6) is absent in the Mahakam River and at

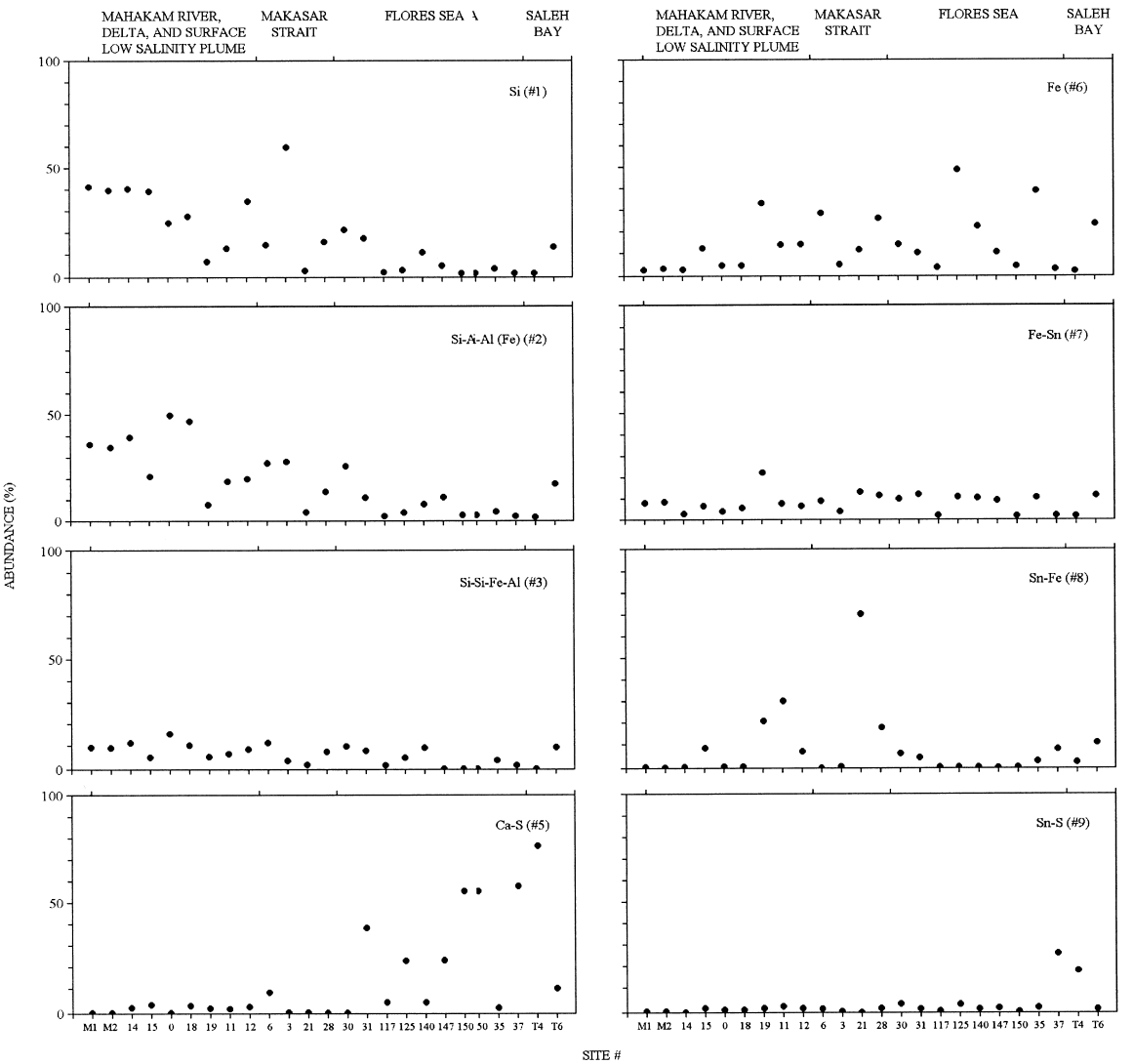

Fig. 6. Abundance distribution of some of the representative particle groups for all the samples studied.

the sites close to its delta. The distribution pattern of this group implies three alternative mechanisms: (1) transportation; (2) precipitation; and (3) passive concentration.

(1) Cassiterite is heavy (specific gravity about 7), and chemically resistant. Nevertheless, small particles (~1 μm) could be transported over long distances.

(2) Romarchite and hydroromarchite most probably result when river-borne dissolved Sn precipitates in seawater (Smith and Burton, 1972; Edwards et al., 1996). Because dissolved Sn was not measured in the Mahakam River, there is no evidence whether precipitation of dissolved Sn plays a role.

(3) In the region much of the rain falls during frequent heavy storms, causing a rapid increase in river discharge whirling up sediment. Although the measurements in the Mahakam River were carried out during the wet season, the presence offshore of Sn-bearing particles might be due to previous events. Also particle sorting might play a role; a small contribution of Sn-bearing particles in the river might

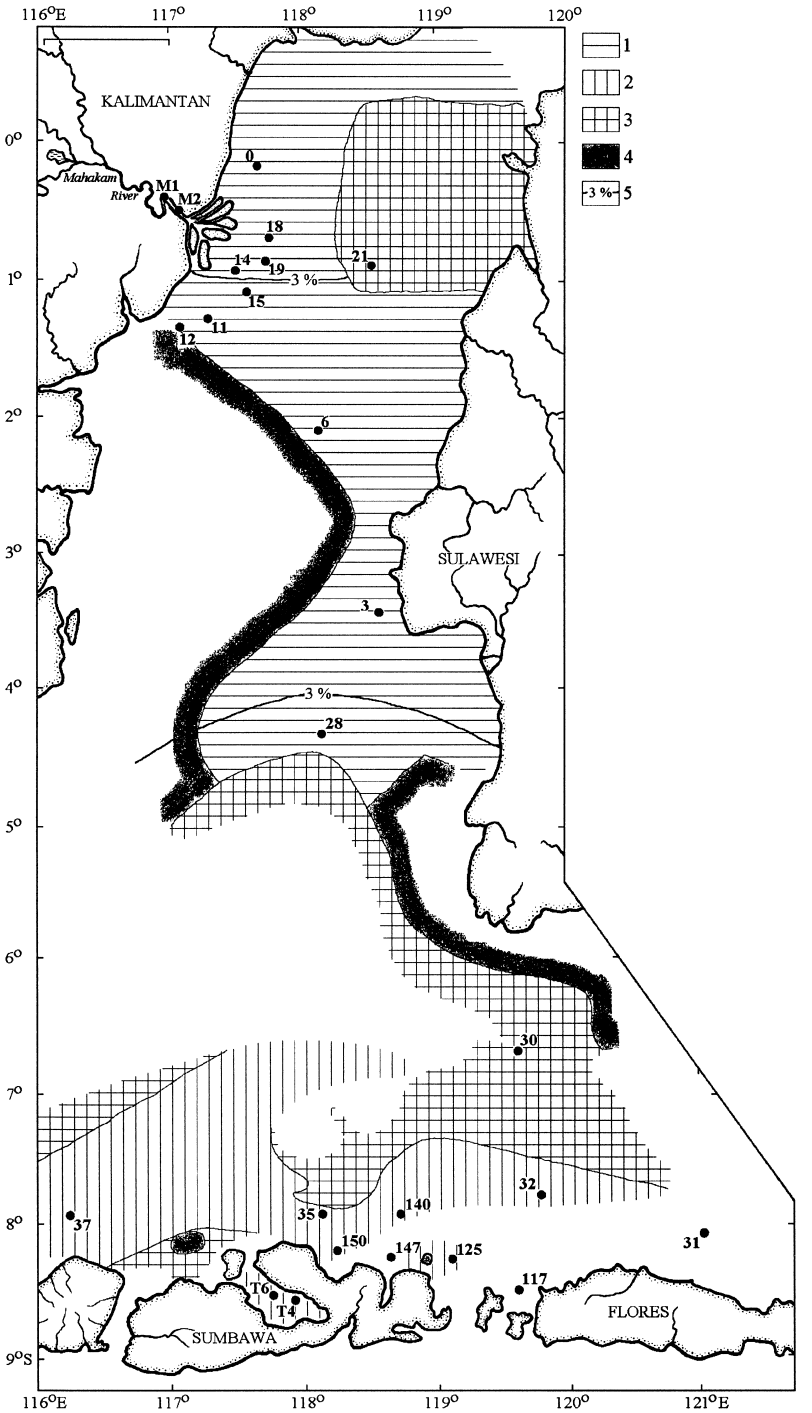

Fig. 7. Distribution of bottom sediment types in the Makasar Strait and Flores Sea (after Neeb, 1943). *1* = terrigenous muds; *2* = volcanogenic sediments; *3* = volcanogenic–terrigenous sediments; *4* = *Globigerina* oozes; *5* = volcanic minerals. The bar in the upper left is 100 km long; dots = sampling stations.

be hidden by the much larger contribution of silica and aluminosilicate particles settling near the shore.

The third tin-rich particle type (#9), composed of *S–Sn particles*, is almost solely found at sites #37 and T4 (Table 3; Fig. 6). Sulphide deposits at the neighbouring islands probably contain tin-bearing sulphides which, on oxidation, can release the tin subsequently supplied to the sea. The high content (36%) of Sn-bearing particles in the westernmost sample site (#37) can be explained by the proximity to the Bali Sea with Sn-rich suspended matter (Van der Sloot et al., 1987).

In summary, the four different sectors of the waters studied have suspended matter with different composition related to: (1) the largely terrigenous input for the Mahakam River–Delta zone; (2) the prevailing volcanic source for the Flores Sea; (3) the specific semi-enclosed environment in the Saleh Bay; (4) the link position of the Makasar Strait between the Indonesian seas and the Pacific, which averages the influence of different suspended matter sources.

3.3. Depth distribution of suspended matter

Not so many drastic differences exist between the average composition of the groups selected for surface suspended matter samples and the composition of the particle types of both depth profiles (Tables 4 and 5). There is a considerable enrichment of FeOOH particles for both sample sets in comparison with the surface samples. Tin-rich particles are restricted to the tin oxide/hydroxide particle type. The absence of the Fe–Sn group, the traces of Sn in some other groups, and the excess of adsorbents (Fe-oxyhydroxides, clays) indicate that the dissolved tin species available for scavenging could hardly have passed the near-shore zone and reached the open Flores Sea (site #32) and Makasar Strait proper (site #6). Another deviation from the surface suspended matter is the presence of five additional particle types, although mostly of minor importance: barite (Ba–S), pyrite (Fe–S), Mn–Fe-oxyhydroxide (Mn–Fe), apatite (P–Fe–Ca–Al) and vivianite (P–Fe).

The different abundance and composition of the aluminosilicate particle types in the two site profiles (Tables 4 and 5) indicate a still appreciable influence of the Mahakam River to the Strait. Vertical distributions of these most abundant groups (Tables 4 and 5; Fig. 8) display a remarkable feature: a sharp increase in their abundance near the bottom. This is more pronounced in the deepest part of the Flores Sea (site #32; Fig. 8A). The bottom few hundred metres of the water column in the deepest parts of the ocean are considerably more turbid than the overlying seawater. This bottom nepheloid layer (BNL) with increased amounts of suspended matter is produced by resuspension of the sediments (McCave, 1986) by lutite flows and turbidity currents. The sites where resuspension takes place appear to coincide with regions where mesoscale eddies develop and surface current velocities are high and variable. Probably, this surface variability and associated turbulence extend to considerable depths, leading to turbulent conditions and erosion of the seafloor. The waters studied (at the onset of the wet season) possess both a high surface current variability (Fig. 2) and eddy kinetic energy which appear to produce a distinct BNL with enhanced suspended matter content near the bottom of the Flores Sea (Eisma et al., 1989, their fig. 7). Consequently, BNL causes the observed high gradients in the vertical abundance distribution of the main particle types near to the bottom (Fig. 8A). Both our present results (Table 5; Fig. 8B) and previous studies on the dispersal of suspended matter in the Makasar Strait (Eisma et al., 1989) do not provide convincing evidence for the development of BNL in the Strait.

Abundances of calcium-rich particles show more variation in the Flores Sea than in the Makasar Strait. The values in the Flores Basin decrease with increasing water depth (Table 4; Fig. 8A), and this is attributed to dissolution of carbonate (coccoliths, foraminifera and pteropods) at depths below the critical CO_3^{2-} ion concentration horizon (lysocline). Low abundances at less than 4000 m depth (Fig. 8A) are due to dilution by more abundant aluminosilicate and Fe-oxyhydroxide groups. Besides Mg-calcite (Ca (Mg) particle type) as in the Flores Sea, the suspended matter from the Makasar depth profile contains pure calcite (group #5, Table 5). Both carbonate groups show no significant variation with depth (Table 5; Fig. 8B), probably because the seafloor at this site is shallower than the lysocline.

The Mn–Fe particle type is only present in small amounts (up to 4%) in the deep parts of the Flores

Table 4
Relative abundance distribution (in %) of the different particle types for the samples from the depth profile (0–5000 m) at station #32

Group	Particle type	0	1000	2000	3000	4000	4800	4900	5000
1	Si–Al–Fe	45 (3) [a]	46 (3)	57 (3)	56 (3)	35 (3)	36 (3)	48 (3)	11 (2)
2	Ca (Mg)	2.2 (0.9)	4 (1)	5 (1)	3 (1)	6 (1)	2.2 (0.9)	5 (1)	0.3 (0.3)
3	Ca–S	8 (2)	9 (2)	9 (2)	1.9 (0.8)	14 (2)	20 (2)	7 (2)	11 (2)
4	Fe	24 (3)	29 (3)	14 (2)	30 (3)	23 (3)	27 (3)	27 (3)	70 (3)
5	Sn (Fe)	16 (2)	8 (2)	12 (2)	5 (1)	16 (2)	9 (2)	6 (1)	5 (1)
6	Ti	3 (1)	4 (1)	2.2 (0.9)	4 (1)	3 (1)	4 (1)	3 (1)	2.4 (0.9)
7	Al	1.5 (0.7)	0.7 (0.5)	0.7 (0.5)	0 (0)	1.1 (0.6)	0.7 (0.5)	0.7 (0.5)	0.7 (0.5)
8	Mn–Fe	0 (0)	0 (0)	0 (0)	0 (0)	0.7 (0.5)	1.1 (0.6)	4 (1)	0.3 (0.3)
9	P–Fe–Ca–Al	0.4 (0.4)	0 (0)	0 (0)	0.8 (0.5)	0 (0)	0.7 (0.5)	0.4 (0.4)	0 (0)

[a] Standard deviation.

Table 5
Relative abundance distribution (in %) of the particle types for the samples from the depth profile (0–2100 m) at station #6

Group	Particle type	0	100	200	400	700	800	1000	1500	2100
1	Si	14 (2) [a]	47 (3)	27 (3)	33 (3)	27 (3)	29 (3)	31 (4)	19 (2)	34 (3)
2	Si–Al (Fe)	30 (3)	34 (3)	26 (3)	26 (3)	27 (3)	27 (3)	23 (4)	20 (2)	34 (3)
3	Fe–Si–Al	12 (2)	5 (1)	7 (2)	11 (2)	6 (1)	8 (2)	7 (2)	7 (2)	8 (2)
4	Ca (Mg)	1 (0.6)	1 (0.6)	1.3 (0.7)	0.4 (0.4)	0.7 (0.5)	1 (0.6)	2 (1)	2 (0.8)	0.7 (0.5)
5	Ca	10 (2)	1.4 (0.7)	0.7 (0.5)	0.4 (0.4)	0.7 (0.5)	0.7 (0.5)	0 (0)	0.3 (0.3)	7 (2)
6	Fe	28 (3)	4 (1)	27 (3)	20 (2)	29 (3)	25 (3)	24 (4)	31 (3)	9 (2)
7	Fe–S	0.3 (0.3)	0.3 (0.3)	0.3 (0.3)	0.7 (0.5)	2 (0.8)	2 (0.9)	2 (1)	4 (1)	1 (0.6)
8	P–Fe	0 (0)	0 (0)	0 (0)	0 (0)	0 (0)	1.4 (0.7)	0.7 (0.7)	0 (0)	0 (0)
9	Sn–Fe	4 (0)	0.3 (0.3)	5 (1)	3 (1)	3 (1)	3 (1)	3 (2)	5 (1)	1.4 (0.7)
10	Ti	2 (1)	4 (1)	1 (0.6)	1 (0.6)	3 (1)	1.4 (0.7)	1 (1)	3 (1)	3 (1)
11	Al	0 (0)	0.7 (0.5)	1.3 (0.7)	3 (1)	1.7 (0.8)	0.4 (0.4)	1 (4)	0.7 (0.5)	1.4 (0.7)
12	Ba–S	0 (0)	3 (1)	3 (1)	3 (1)	1 (0.6)	2 (0.9)	3 (2)	8 (2)	1.4 (0.7)

[a] Standard deviation.

Basin (Table 4; Fig. 8A). This points to a source in the sediments, which is not surprising since the sediments in the Flores Sea (Eisma, 1985) as well as in the adjacent basins (De Lange et al., 1989; Helder, 1989) have a thin, brown MnO_2-enriched surface layer. Erosion by bottom currents causes these particles to be present in the BNL (Fig. 8A). They could also be formed in near-bottom seawater from the upward flux of dissolved Mn^{2+} from the sediments. Oxidation to Mn^{4+} is slow below pH of 8.5, but suspended particles, e.g. Fe-oxyhydroxides or Mn-oxides, accelerate the oxidation markedly.

The peak of the Fe-oxyhydroxide abundance near the seafloor (Fig. 8A) has the same origin. The kinetics of the Fe^{2+} oxidation in seawater are rapid above $pH = 6$ and therefore reduced iron introduced into seawater will be rapidly removed as Fe-oxyhydroxides. The high abundance (30%) of the suspended iron phases in the Flores Sea indicates a fairly high flux of dissolved iron into the basin.

Silica particle type, partly characterised by a biogenous fraction (diatoms and radiolaria), is more resistant to dissolution and bacterial consumption and does not exhibit prominent vertical variations in the Makasar Strait (Fig. 8B).

Barite ($BaSO_4$) particles, which are found to be a universal component of suspended matter in the ocean, are mainly the result of biochemical processes (Dehairs et al., 1980). The nutrient-like vertical profile of suspended barium in the upper 400 m of the Makasar Strait water column (Fig. 8B) suggests a biogenic control of barite formation. The barite maximum at 1500 m is also of a biogenic nature: a tongue of organic-rich suspended matter spreads through these water levels (Eisma et al., 1989, their fig. 6). Some of the barite dissolves at depth in the

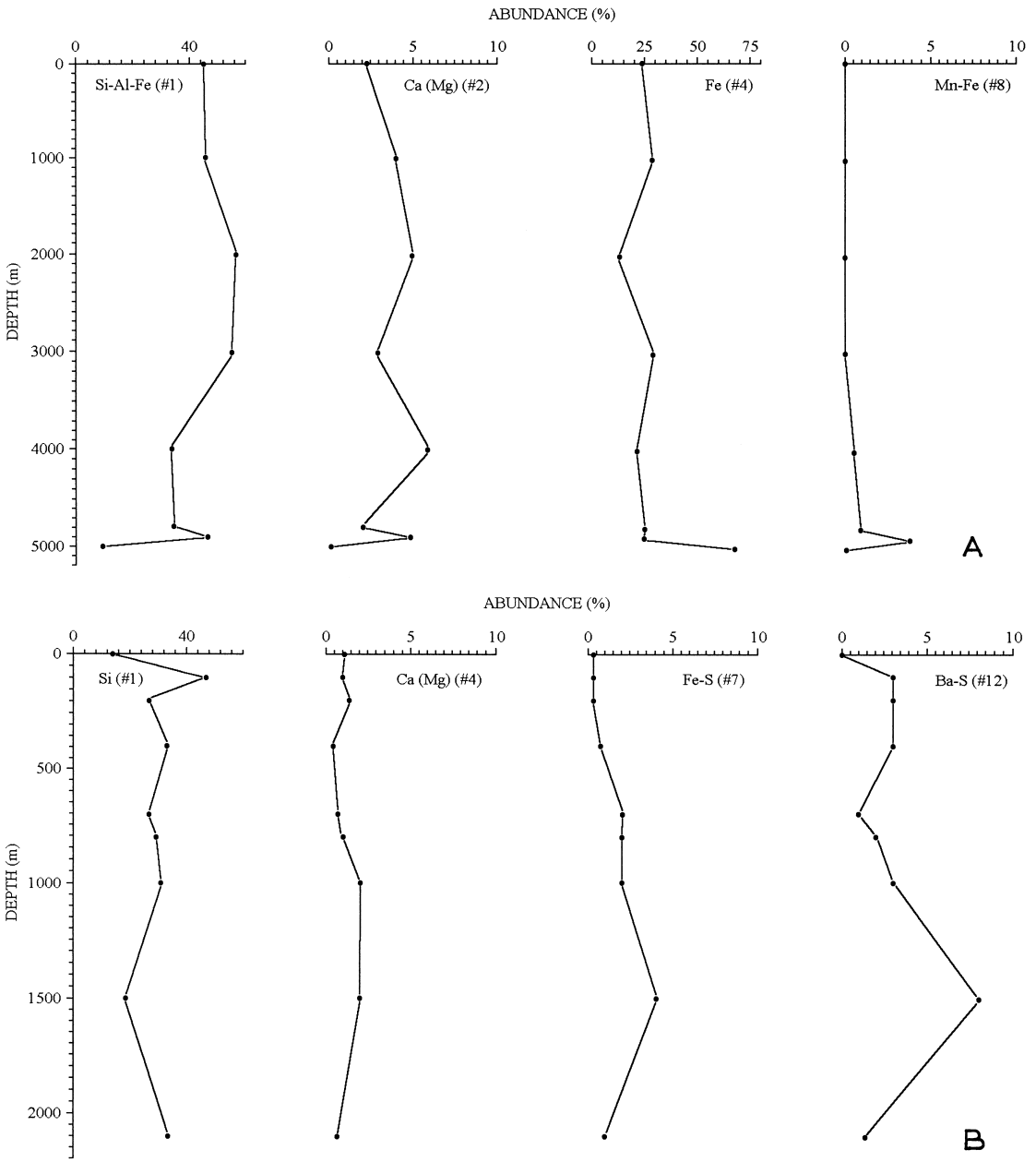

Fig. 8. Relative abundance distribution with depth for some of the representative particle types for stations (A) #32 and (B) #6.

water column and its abundance decreases towards the floor of the Strait (Fig. 8B).

Framboidal pyrite particles as well as barite crystals were frequently observed both in the suspended matter (our SEM studies) and in the sediments of the Strait (Eisma et al., 1989). The vertical distribution pattern of the pyrite particle type (Fe–S, Fig. 8B) suggests that it originates from particulate organic matter. Probably, the framboidal pyrite formation begins in the water column under reducing microenvironments in organic-rich suspended matter plumes.

The high bioproduction in the euphotic water layer is responsible not only for barite and pyrite formation but for the presence of two other quite exotic particle types: apatite (site #32, Table 4) and vivianite (site #6, Table 5).

Along the vertical profiles, tin-bearing particle types behave conversely to the main suspended matter contributors: silicates, aluminosilicates, Fe-oxyhydroxides (Tables 4 and 5), and do not show any remarkable features.

4. Conclusions

Thirteen particle types describe the composition of suspended matter from the basins studied. The bulk of suspended matter consists of silicates, aluminosilicates and Fe-oxyhydroxides. Four different sectors of the studied waters have suspended matter with different composition related to: (1) the largely terrigenous input for the Mahakam River–Delta zone; (2) the prevailing volcanic source for the Flores Sea; (3) the specific semi-enclosed environment in the Saleh Bay, resulting in the formation of a two-layered stratified water body; (4) the link position of the Makasar Strait between the Indonesian seas and the Pacific, which averages the influence of different suspended matter sources.

Suspended matter of the region contains fairly high levels of tin-bearing particles which on the basis of their composition fall into three groups: (1) tin oxide/hydroxides (Sn–Fe); (2) iron-oxyhydroxides with adsorbed tin (Fe–Sn); and (3) tin hydroxysulphates (S–Sn). The tin oxide/hydroxide group most probably encompasses: ultra-fine ($\sim$1 μm) cassiterite particles, delivered either from the land frame of the basins mainly by river currents or from far-away sources by sea currents; romarchite and hydroromarchite presumably precipitated from dissolved tin species during the mixing of river waters with seawater. Two other pathways for dissolved tin are: (1) to be scavenged by Fe-oxyhydroxides; and (2) to precipitate as a mixed oxidation state or as tin hydroxysulphates. It is concluded that dissolved and suspended tin originate from local as well as remote sources where the natural mobilisation of tin is sometimes accelerated by human activities.

The depth distribution of suspended particle types is governed by: (1) the bottom nepheloid layer and lysocline in the Flores Sea; (2) the high bioproduction in the euphotic water layer and the vertical distribution of organic matter in the Makasar Strait.

Acknowledgements

We are much indebted to Captain De Jong of RV *Tyro* and Captain Müller of RV *Sonne* and their crews for their co-operation during the cruises and the pleasant stay on board. Thanks go to W.K. Fletcher and H.S. Stoynov (both from the University of British Columbia, Canada), and G. Eskenazy (University of Sofia, Bulgaria) for providing the literature and for helpful discussions. An anonymous reviewer and J. Van Bennekom provided helpful comments, which improved the manuscript. The University of Antwerp is thanked for the provision of a post-doctoral fellowship to V.M. Dekov.

References

Bernard, P., Van Grieken, R., Eisma, D., 1986. Classification of estuarine particles using automated electron microprobe analysis and multivariate techniques. Environ. Sci. Technol. 20, 467–473.

Blundel, S., Evans, C., 1990. Organotin compounds. In: Hutzinger, O. (Ed.), Handbook of Environmental Chemistry, 3. Springer, Berlin, pp. 1–126.

Brewer, P.G., 1975. Minor elements in sea water. In: Riley, J.P., Skirrow, G. (Eds.), Chemical Oceanography. Academic Press, London, pp. 415–496.

Chansang, H., 1988. Coastal tin mining and marine pollution in Thailand. Ambio 17, 223–228.

Curray, J.R., 1989. The Sunda Arc: a model for oblique plate convergence. Neth. J. Sea Res. 24, 131–140.

Degens, E.T., Buch, B., 1989. Sedimentological events in Saleh Bay, off Mount Tambora. Neth. J. Sea Res. 24, 399–404.

Dehairs, F., Chesselet, R., Jedwab, J., 1980. Discrete suspended particles of barite and the barium cycle in the open ocean. Earth Planet. Sci. Lett. 49, 528–550.

De Lange, G.J., Middelburg, J.J., Poorter, R.P., Shofiyah, S., 1989. Ferromanganese encrustations on the seabed west of Misool, eastern Indonesia. Neth. J. Sea Res. 24, 541–553.

Duinker, J.C., Everaarts, J.M. (Eds.), 1989. River inputs into ocean systems. Proceedings of Snellius-II Symposium. Neth. J. Sea Res. 23, 353–527.

Edwards, R., Gillard, R.D., Williams, P.A., 1992. The stabilities of secondary tin minerals: abhurite and its relationships to Sn

(II) and Sn (IV) oxides and oxyhydroxides. Mineral. Mag. 56, 221–226.

Edwards, R., Gillard, R.D., Williams, P.A., 1996. The stabilities of secondary tin minerals, part 2. The hydrolysis of tin (II) sulfate and the stability of $Sn_3O(OH)_2SO_4$. Mineral. Mag. 60, 427–432.

Eisma, D., 1985. Theme I Geology and geophysics of the Banda Arc and adjacent areas. The Snellius-II expedition progress report, November 1984, pp. 1–28.

Eisma, D., 1990. Dispersal of Mahakam River suspended sediment in Makasar Strait, Indonesia. In: Ittekkot, V., Kempe, S., Michaelis, W., Spitzy, A. (Eds.), Facets of Modern Biogeochemistry. Springer, Heidelberg, pp. 127–146.

Eisma, D., Kalf, J., Karmini, M., Mook, W.G., Van Put, A., Bernard, P., Van Grieken, R., 1989. Dispersal of suspended matter in Makasar Strait and the Flores Basin. Neth. J. Sea Res. 24, 383–398.

Eisma, D., Van Put, A., Van Grieken, R., 1992. Distribution and composition of suspended matter around Sumbawa Island, Indonesia. Mitt. Geol. Paläontol. Inst. Univ. Hamburg 70, 137–147.

Forgy, E.W., 1965. Cluster analysis of multivariate data: efficiency versus interpretability of classifications. Biometrics 21, 768.

Galvin, R.M., 1996. Occurrence of metals in waters: an overview. Water S.A. 22, 7–18.

Gucer, S., Van Vaeck, L., Adams, F., 1989. Characterization of graphite furnace produced aerosols by laser microprobe mass spectrometry and electron microprobe analysis. Spectrochim. Acta B 44, 1021–1039.

Hamaguchi, H., Kuroda, R., 1978. Tin. Behaviour during weathering and rock alteration. In: Wedepohl, K.H. (Ed.), Handbook of Geochemistry. Springer, Berlin, II/4, 50-G-I.

Hamaguchi, H., Kuroda, R., Onuma, N., Kawabuchi, K., Mitsubayashi, T., Hosohara, K., 1964. The geochemistry of tin. Geochim. Cosmochim. Acta 28, 1039–1053.

Helder, W., 1989. Early diagenesis and sediment–water exchange in the Savu Basin (Eastern Indonesia). Neth. J. Sea Res. 24, 555–572.

Heydemann, A., 1969. Tables. In: Wedepohl, K.H. (Ed.). Handbook of Geochemistry. Springer, Berlin, I, pp. 376–412.

Hoekstra, P., Nolting, R., Van der Sloot, H., 1989. Supply and dispersion of water and suspended matter of the rivers Solo and Brantas into the coastal waters of East Java. Neth. J. Sea Res. 23, 517–527.

Katili, J.A., 1989. Review of past and present geotectonic concepts of Eastern Indonesia. Neth. J. Sea Res. 24, 103–129.

Kennish, M.J. (Ed.), 1994. Practical Handbook of Marine Science (2nd ed.). CRC Press, Boca Raton, FL, 566 pp.

Kuo-Chin, S., 1995. The mineral industry of Indonesia. In: Minerals yearbook; area reports; International 1995 mineral industries of Asia and the Pacific, III. U.S. Geological Survey, Reston, VA, pp. 79–86.

Lal, D., 1977. The oceanic microcosm of particles. Science 198, 997–1009.

Li, Y.-H., 1981. Geochemical cycles of elements and human perturbation. Geochim. Cosmochim. Acta 45, 2073–2084.

Lisitzin, A.P., 1972. Sedimentation in the World Ocean. Soc. Econ. Mineral. Paleontol. Spec. Publ. 17, 218 pp.

Massart, D.L., Kaufman, L., 1983. The Interpretation of Analytical Data by the Use of Cluster Analysis. Wiley, New York, 237 pp.

McCave, I.N., 1986. Local and global aspects of the bottom nepheloid layers in the world ocean. Neth. J. Sea Res. 20, 167–181.

Milliman, J.D., Meade, R.H., 1983. World-wide delivery of river sediment to the oceans. J. Geol. 91, 1–21.

Neeb, G.A., 1943. The Composition and Distribution of the Samples. Snellius-Expedition 1929–1930. E.J. Brill, Leiden, V 3, II, 268 pp.

Nolting, R., Hutagalung, H., Moelyadi Moelyo, D., 1989. Distribution of dissolved and particulate minor and major elements in the river and coastal environment of East Java during the Snellius-II expedition. Neth. J. Sea Res. 23, 387–402.

Otten, Ph., Bruynseels, F., Van Grieken, R., 1986. Nitric acid interaction with marine aerosols sampled by impaction. Bull. Soc. Chim. Belg. 95, 447–451.

Ottmann, F., Shi, W., 1988. Syngenetic origin of gypsum crystals bearing bacterial calcite neoformation, discovered within suspended matter in the Loire. C.R. Acad. Sci. Paris 306, 803–808.

Pei, R., Qiu, X., 1995. Metallogeny and evolution of the Asia–Australia W–Sn metallogenic belt on the western Pacific rim. In: Mauk, J.L., St. George, J.D. (Eds.), Exploring the Rim. Proceedings of the 1995 PACRIM Congress, Australasian Institute of Mining and Metallurgy, Parkville, 9/95, pp. 459–463.

Postma, H. (Ed.), 1988. Ventilation of deep-sea basins. Proceedings of Snellius-II Symposium. Neth. J. Sea Res. 22, 315–413.

Ransom, B., Kim, D., Kastner, M., Wainwright, S., 1998. Organic matter preservation on continental slopes: importance of mineralogy and surface area. Geochim. Cosmochim. Acta 62, 1329–1345.

Riley, J.P., Chester, R., 1971. Introduction to Marine Chemistry. Academic Press, London, 465 pp.

Shimizu, K., Ogata, N., 1963. Determination of trace of tin in common salt with phenylfluorone. Bunseki Kagaku 12, 526–531.

Smith, J.D., Burton, J.D., 1972. The occurrence and distribution of tin with particular reference to marine environments. Geochim. Cosmochim. Acta 36, 621–629.

Stumpfl, E.F., Clark, A.M., 1965. Electron-probe microanalysis of gold–platinoid concentrates from southeast Borneo. Trans. Inst. Min. Metall. 74, 933–946.

Supriyadi, U.N., 1996. Tin exploration in Indonesia; problems and solution. In: Jones, H. (Chairperson), Diversity; the Key to Prosperity. Australasian Institute of Mining and Metallurgy, Parkville, 1/96, pp. 385–391.

Van Bennekom, A.J., 1988. Deep-water transit times in the eastern Indonesian basins, calculated from dissolved silica in deep and interstitial waters. Neth. J. Sea Res. 22, 341–354.

Van Borm, W.A., Adams, F.C., 1988. Cluster analysis of electron microprobe analysis data of individual particles for source

apportionment of air particulate matter. Atmos. Environ. 22, 2297–2307.

Van der Land, J. (Ed.), 1989. Coral Reefs. Proceedings of Snellius-II Symposium. Neth. J. Sea Res. 23, 83–238.

Van der Sloot, H.A., Hoede, D., Wijkstra, J. (Eds.), 1987. On the occurrence of tungsten, tin, silver and gold in River Solo and waters around Java. Rep. ECN-87-104, 1–13.

Van Hinte, J.E., Van Weering, Tj.C.E., Fortuin, A.R. (Eds.), 1989a. Geology and geophysics of the Banda Arc and adjacent areas, part 1. Proceedings of Snellius-II Symposium. Neth. J. Sea Res. 24, 93–381.

Van Hinte, J.E., Van Weering, Tj.C.E., Fortuin, A.R. (Eds.), 1989b. Geology and geophysics of the Banda Arc and adjacent areas, part 2. Proceedings of Snellius-II Symposium. Neth. J. Sea Res. 24, 383–622.

Wouters, L., Bernard, P., Van Grieken, R., 1988a. Characterization of individual estuarine and marine particles by LAMMA and EPXMA. Int. J. Environ. Anal. Chem. 34, 17–29.

Wouters, L., Van Grieken, R., Linton, W., Bauer, C., 1988b. Discrimination between coprecipitated and adsorbed lead on individual calcite particles using Laser Microprobe Mass Analysis. Anal. Chem. 60, 2218–2220.

Wyrtki, K., 1961. Physical oceanography of the southeast Asian waters. Naga Rep. 2, 1–195.

Yim, W., 1981. Geochemical investigations on fluvial sediments contaminated by tin-mine tailings, Cornwall, England. Environ. Geol. 3, 245–256.

Zijlstra, J.J., Baars, M.A., Cadée, G.C. (Eds.), 1990. Pelagic Systems. Proceedings of Snellius-II Symposium. Neth. J. Sea Res. 25, 423–650.